GEOPHYSICAL RESEARCH LETTERS, VOL. 35, L02604, doi:10.1029/2007GL032440, 2008

Click Here for Full Article

Upwelling off the west coast of Hainan Island in summer: Its detection and mechanisms

Xingang Lü,[1,2,3,4] Fangli Qiao,[2,4] Guansuo Wang,[2,4] Changshui Xia,[2,4] and Yeli Yuan[2,4]

Received 23 October 2007; revised 25 November 2007; accepted 10 December 2007; published 18 January 2008.

[1] The summertime upwelling off the west coast of Hainan Island is newly detected by satellite remote sensing sea surface temperature, and confirmed by both historical field observations and numerical modeling. Furthermore, numerical experiments are conducted to gain understanding of the upwelling mechanisms. A tidal mixing front (TMF) is identified as the vital factor triggering the formation of the upwelling. The baroclinic pressure gradient force, which stems from the intense density difference across the TMF, causes a frontal-scale circulation at the TMF. As a result, upwelling appears as a branch of this circulation. The southwest monsoon induces downwelling, which competes with the front-induced upwelling. Climatologically, the upwelling dominates and can reach about 5 m below the sea surface above the slope bottom. In calm weather with no or weak winds, it is expected that the upwelling can reach all the way to the sea surface. **Citation:** Lü, X., F. Qiao, G. Wang, C. Xia, and Y. Yuan (2008), Upwelling off the west coast of Hainan Island in summer: Its detection and mechanisms, *Geophys. Res. Lett.*, *35*, L02604, doi:10.1029/2007GL032440.

1. Introduction

[2] Hainan, an island covering an area of about 33,920 km^2, is located at the northwest corner of the South China Sea (SCS), and separated from China mainland by Qiongzhou Strait. To the west of Hainan lies the Gulf of Tonkin (GT, also Beibu Gulf), which is a semi-enclosed shallow bay bounded by Vietnam and south China (Figure 1). The general circulation in SCS, including the waters around Hainan Island, is susceptible to the monsoon, which prevails all year round with the alternation of northeasterly winds in winter and southwesterly winds in summer.

[3] The pioneering investigation of the coastal upwelling around Hainan Island can be traced back more than 40 years (Guan and Chen, unpublished report, 1964). The areas off the east and the northeast coasts of Hainan Island are believed to be the centers of the upwelling. Almost all the reported studies on the upwelling around the Island have focused on these two regions [e.g., *Han et al.*, 1990; *Li*, 1990; *Deng et al.*, 1995; *Chai et al.*, 2001]. The upwelling off the east coast of Hainan usually appears and intensifies in boreal summer when the southwest monsoon prevails, and is commonly accepted to be induced mainly by the wind-driven Ekman effects. From June to August, the monsoon is stable and generally parallel to the coastline (Figure 2), resulting in a net upper ocean transport toward the open sea and the consequent divergence along the coast, which permits the drawing up of the cold deep water to maintain mass conservation.

[4] In contrast, the coastal water off the west coast of Hainan Island (WCH) has never been a highlighted spot for upwelling investigation. In the study of Chlorophyll *a* in GT, *Tang et al.* [2003] noticed the cold water along WCH in the satellite sea surface temperature (SST) image of 11 August 2000, without giving a detailed explanation. At first sight, the upwelling off WCH seems to be unlikely since the direction of the summer prevailing winds is generally parallel to WCH (Figure 2), which should lead to coastal downwelling. However, if mechanisms other than Ekman transport are involved, it is still possible for the upwelling off WCH to occur.

[5] In this paper, evidence for the persistent occurrence of the upwelling off WCH in summer will be presented by combining remote sensing SST data, historical cruise observations, and numerical modeling. Furthermore, the mechanisms causing the upwelling will be discussed based on numerical experiments.

2. Data and Methodology

[6] Since the vertical velocity is too weak to be measured directly by instrumental means, upwelling is commonly detected through an analysis of the distribution patterns of geophysical or geochemical parameters such as the sea water temperature, dissolved oxygen (DO), and nitrates.

2.1. AVHRR-Derived SST

[7] The satellites of National Oceanic and Atmospheric Administration (NOAA) provide SST measurements from the Advanced Very High Resolution Radiometer (AVHRR). Among the varieties of SST products, the NSIPP (NASA Seasonal to Interannual Prediction Project) AVHRR Pathfinder SST monthly climatology [*Casey and Cornillon*, 1999] was chosen in this study. This dataset was created using daily averaged Pathfinder SST over monthly periods from 1985 to 1997 at 9.28 km spatial resolution.

[8] An advantage of using climatological SST is that the data have been averaged over a long period of time which minimizes noise, thus providing better information. In addition, the climatology merges large quantities of data, and therefore maximizes the coverage of cloud-free areas.

2.2. Historical Cruise Observation

[9] Field data obtained from a joint Chinese-Vietnamese investigation are used to analyze the vertical distributions of

[1]Institute of Oceanology, Chinese Academy of Sciences, Qingdao, China.
[2]First Institute of Oceanography, State Oceanic Administration, Qingdao, China.
[3]Graduate University of the Chinese Academy of Sciences, Beijing, China.
[4]Key laboratory of Marine Science and Numerical Modeling (MASNUM), State Oceanic Administration, Qingdao, China.

0094-8276/08/2007GL032440$05.00

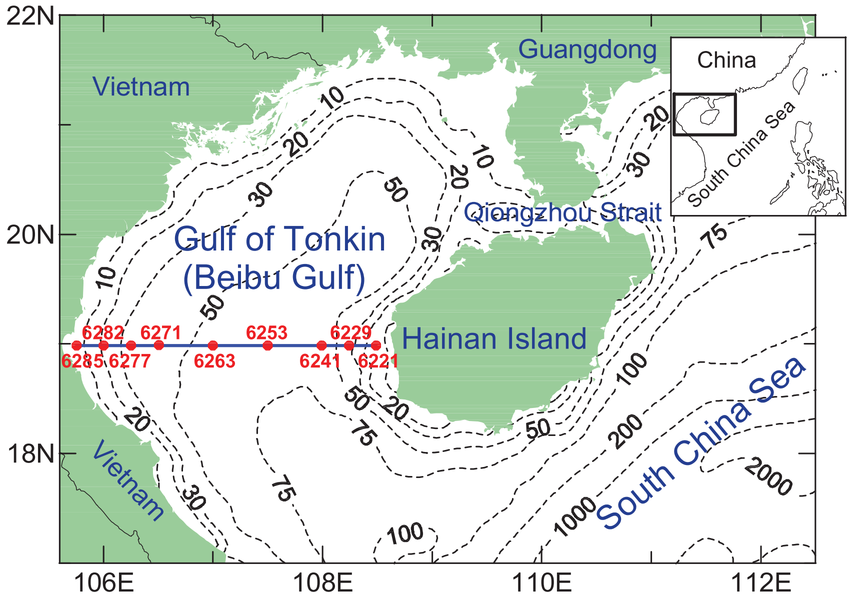

Figure 1. Map of the study area. The relative location is shown as a solid square in the inset. The dashed lines represent isobaths in meters. The blue line and red dots show the cruise route and stations along 19°N.

the upwelling signals as a supplement to the satellite SST, which provides only sea surface information. The joint survey, which was conducted from December 1959 to December 1960, has been the first and the largest scale multi-disciplinary investigation undertaken in GT until now.

[10] The cruises were carried out by R/V *Haidiao 0010*, *Nanyu 228*, *Nanyu 402*, and *Hanggong 01*, and covered the entire GT with a total of 88 stations along 16 transects. Discrete seawater samples were collected from the depths of 0, 5, 10, 15, 20, 25, 35, 50, 75 m and the bottom layer using

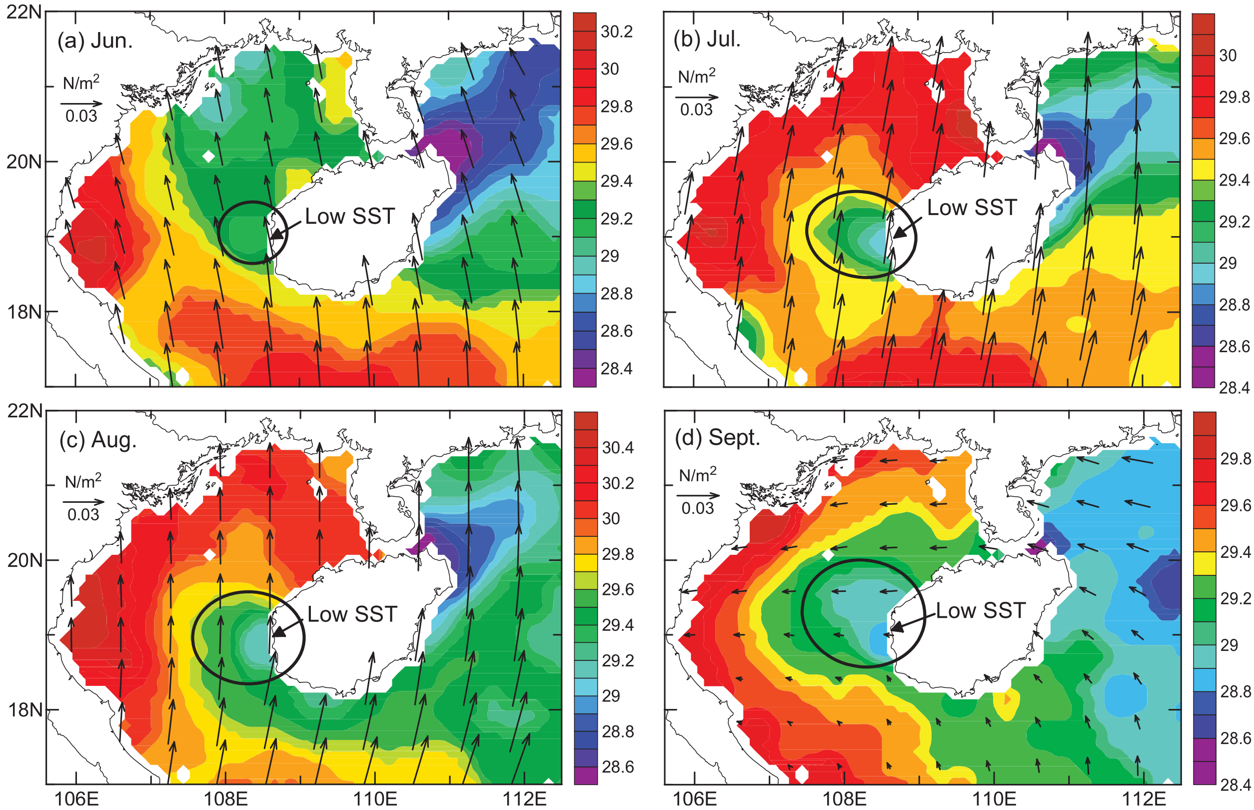

Figure 2. NOAA AVHRR SST (°C) climatology for (a) June, (b) July, (c) August, and (d) September superimposed with monthly wind stress vectors (N m^{-2}) of the corresponding month from Comprehensive Ocean-Atmosphere Data Set. The black circles denote the low SSTs off WCH.

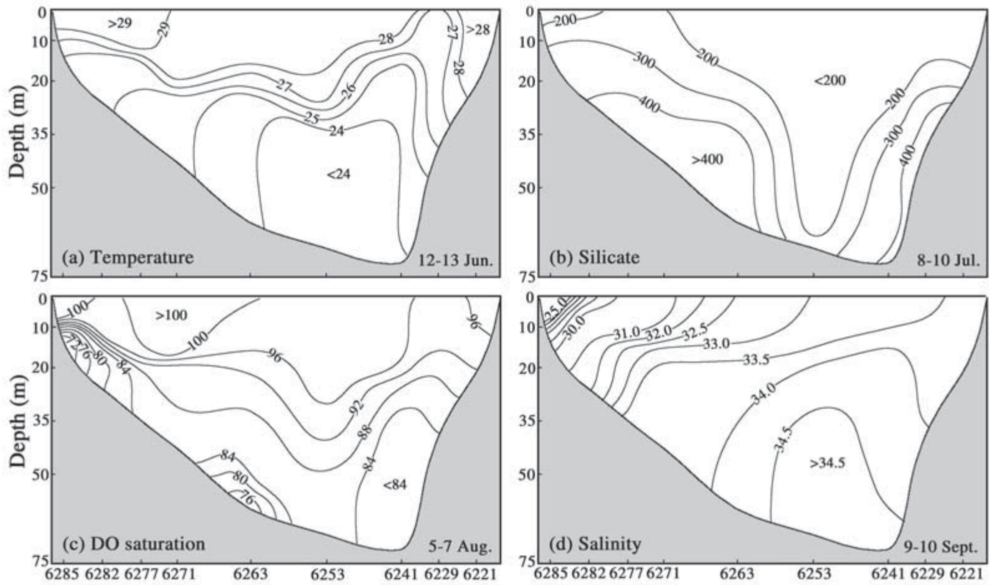

Figure 3. Vertical distributions of (a) sea temperature (°C), (b) silicate (μg L^{-1}), (c) DO saturation (mL L^{-1}), and (d) salinity on cross section along 19°N (see Figure 1 for the transect location). The observation dates are marked on each figure.

1000-ml reversing samplers. Water temperature was measured by protected reversing thermometers and bathythermographs (BT). The salinity was calculated by the Knudsen formula based on the chlorinity measurement. The chlorinity was determined by means of Mohr's silver nitrate titration method, DO by Winkler method, and silicate by Dienert-Wandenbulcke method. The precision of temperature measurement was ±0.02°C. The precisions of the chlorinity and DO measurements were 0.02‰ and ±0.03 mL L^{-1}, respectively, based on duplicate sample analyses.

2.3. Numerical Modeling

[11] An improved version of the Prince Ocean Model (POM) [*Blumberg and Mellor*, 1987], MASNUM wave-tide-circulation coupled model [*Qiao et al.*, 2004], is used to simulate the three dimensional circulation in GT. The model covers the northwest Pacific (0°–50°N, 99°–150°E) with a horizontal resolution of 1°/8 × 1°/8 and 21 sigma levels in the vertical. The values of sigma coordinate are 0.000, −0.002, −0.004, −0.008, −0.017, −0.033, −0.067, −0.133, −0.200, −0.267, −0.333, −0.400, −0.467, −0.533, −0.600, −0.667, −0.733, −0.800, −0.867, −0.933, and −1.000 from the surface to the bottom. Comprehensive physical processes, including monsoon forcing, heat fluxes, four main tide constituents (M_2, S_2, K_1, and O_1), and open boundary forcing, are taken into consideration. Details of the model configuration were given by *Xia et al.* [2006].

[12] Besides the standard modeling (the Control Run), two experiments, Case NoT and Case NoW, are designed and carried out to examine the roles of the tidal forcing and the monsoon, respectively, in the formation of the upwelling. In Case NoT, the tides are excluded from the model, while other physical processes are kept unchanged; in Case NoW, similarly, the only modification to the model is removing the wind forcing in the study area (17°–22°N, 105.6°–112.5°E, as shown in Figure 1).

3. Evidence of Upwelling

3.1. Evidence From Remote Sensing Data

[13] In the AVHRR monthly SST images from June to September, the most conspicuous feature is the coldest water off the northeast coast of Hainan Island (Figure 2). This low SST area has been verified by field observations in different years by different researchers [e.g., *Han et al.*, 1990; *Li*, 1990; *Deng et al.*, 1995]. Although this cold water is not the focus of this study, its confirmation by the field surveys lends credit to the reliability of the satellite SST data.

[14] Another striking feature of Figure 2 is the persistence of a cold center off WCH. After appearing in June, the cold water off WCH grows quickly with the strengthening SST gradient: within the black circles as shown in Figure 2, the SST amplitudes grow from 0.15 °C in June to 0.6 °C in July. Then the cold water decays in September, and vanishes in October. July and August could be regarded as a mature stage of the development of the low SST area, when the largest SST gradient reaches about 0.01°C per kilometer. The cold water is closely confined to the coast in July, and spreads to its widest extent in September. Using climatological data, we note that the monthly SST averaged over 13 years will always be higher (lower) than the minimum (maximum) SST in the annual cycle. In the real time satellite images, it is reasonable to expect even stronger SST gradients off WCH. In this connection, the upwelling signals detected from Figure 2 could be regarded as persistent and stable ones.

3.2. Evidence From Cruise Observation

[15] Again, pronounced upwelling was clearly seen on the cross section along 19°N from the joint Chinese-Vietnamese survey (Figure 3). Upwelling could easily be

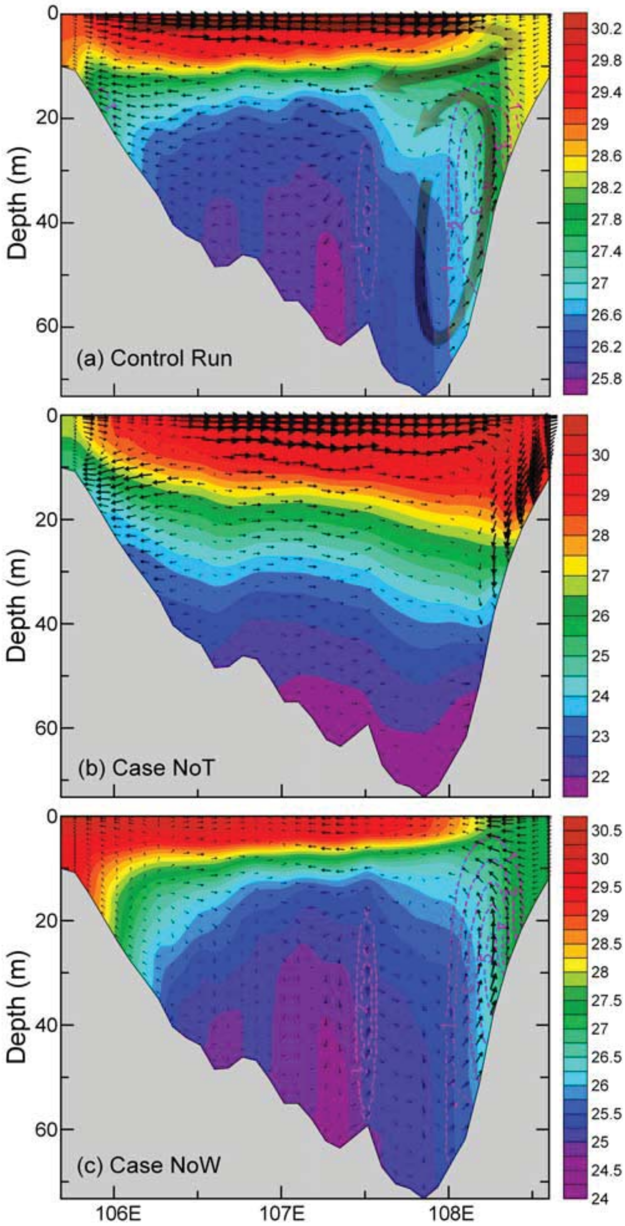

Figure 4. Numerically modeled vertical distributions of *u*-*w* vectors superimposed on temperature (°C) along 19°N in July for (a) Control Run, (b) Case NoT, and (c) Case NoW. In Figures 4a and 4c, the dashed magenta contours showing upwelling velocity starts from 1×10^{-5} m s^{-1} with interval of 1×10^{-5} m s^{-1}. In Figure 4a, the upper massive curve with arrow indicates the wind-driven downwelling, while the bottom one denotes frontal circulation. The vertical velocity has been amplified 1000 times for plotting vectors.

determined by the upward distortion of the parameter contours off WCH. The contours were uplifted along the eastern slope (Hainan side), resulting in a severe decrease in temperature and DO, and an increase in salinity and SiO_3 near the shelf slope. The prominent dome structure of the isopleths indicated the upwelling movement between station 6241 and 6221. The upwelling was extraordinarily evident during 12–13 June and 5–7 August. Not only did upward curvature of isotherms occur (Figure 3a), but the upward movement outcropped at the surface: the 27°C isotherm was uplifted from 33 m depth to the surface, and the originally smooth isopleth was distorted into a distinct arch. The thermocline was elevated from west to east, and ventilated off WCH. The distribution of iso-DO line of 96 mL L^{-1} showed a similar pattern (Figure 3c). In Figures 3b and 3d, upwelling could also be discerned at least below 10 m.

3.3. Evidence From Numerical Model

[16] The model results provide additional evidence of the presence of upwelling off WCH. Besides the two well-known cold water regions in the coastal areas east and northeast of Hainan Island, respectively, the low SST center off the west coast, plus another minor cold water mass at (109.1°E, 18.2°N) (see Figure 2c), are also reproduced successfully by the model. A comparison between the modeled SST in August (figure not shown) and the one from remote sensing suggests that the model performs well. It is therefore justifiable to conduct further numerical experiments to explore the physics of the upwelling.

4. Upwelling Mechanisms

[17] The individual results from the two experiments are compared with those of the Control Run in order to determine the critical dynamical factors affecting the upwelling. In the Control Run, very clear upwelling can be found along the bottom slope off WCH, and the maximum upwelling velocity exceeds 4×10^{-5} m s^{-1} (Figure 4a). The temperature patterns, especially the upward curvature of the isotherms, are comparable to those observed, shown in Figure 3a. In sharp contrast, the upwelling disappears completely, but strong downwelling occurs, when tides are excluded from the model (Figure 4b). The absence of winds in Case NoW brings about significant enhancement of upwelling (Figure 4c). These results suggest that tides play a key role in inducing upwelling, whereas the influence of the monsoon forcing acts in the opposite way.

4.1. Effects of Tidal Mixing

[18] *Lü et al.* [2006] proposed a "frontal upwelling" mechanism for the Zhejiang coastal upwelling. This mechanism is used to shed light on the formation of the upwelling in this study.

[19] Tidal mixing is the trigger of the upwelling off WCH. The computation of the maximum possible tidal currents shows that the most tidally energetic area coincides with the region of upwelling (figure not shown). In these coastal waters with strong tidal signals, the shallow water is well-mixed from the bottom to the surface, attaining high temperature in summer due to solar radiation. In the deeper area along the slope, the bottom water up to 30 m (Figure 4a) is mixed by the tide-induced turbulence, whereas the upper water remains stratified. Naturally, a tidal mixing front (TMF) is sandwiched along the slope between the vertically homogeneous shallow and warmer water, and the stratified colder water on the deep side. *Lü et al.* [2006] have demonstrated that along the bottom slope where a sharp TMF exists, the lowest order momentum balance is between the baroclinic pressure gradient force (PGF) and the vertical diffusion term. The baroclinic PGF is strong enough to stimulate a frontal-scale circulation, with a clear

upwelling branch, across the front (see the schematic massive arrow in Figure 4a).

[20] *Hu et al.* [2003] investigated the fronts in GT, and reported the existence of typical TMF off WCH by using the Simpson-Hunter index [*Simpson and Hunter*, 1974]. The location of TMF [see *Hu et al.*, 2003, Figure 2b] agrees perfectly with the area of upwelling detected in this study. Their work lends additional support to the frontal upwelling mechanism described above.

4.2. Effects of Monsoon Forcing

[21] Undoubtedly, the southwest monsoon induces downwelling off WCH in accordance with Ekman theory, which is also confirmed by the model (see the upper massive arrow in Figure 4a). Therefore the upwelling off WCH is in fact a result of two competing forces, namely, the wind-driven downwelling and the frontal upwelling. Model results illustrate that upwelling is dominant. As Figure 4a shows, the upwelled water develops from the bottom and goes up approximately to a depth of 5 m below the sea surface (note that the minimum contour value in Figures 4a and 4c is 1×10^{-5} m s^{-1} rather than zero). The upwelling strengthens remarkably and reaches the sea surface once winds are removed from the model (Figure 4c). The averaged upwelling velocity in Case NoW is 2.1×10^{-5} m s^{-1}, which is about 20% higher than that of Control Run.

5. Conclusions

[22] Despite the prevailing southwest monsoon in summer, there still exists persistent upwelling off the west coast of Hainan Island. This upwelling is detected and verified by a combination of satellite SST, cruise observation, and numerical modeling.

[23] The upwelling off WCH is induced by tidal mixing front. In the Gulf of Tonkin, the strongest tidal currents, which directly result in strong TMF along the slope, are generally coincident with the upwelling location. The density difference between the two sides of TMF results in large baroclinic PGF which drives a secondary circulation at the front, so that the upwelling branch appears on the slope. Downwelling driven by the summer monsoon occurs together with the TMF-induced upwelling. In a climatological sense, upwelling is dominant and controls the water column from the slope bottom to about 5 m below the surface. Based on the results from numerical experiments, it is reasonable to infer that under calm atmospheric conditions the upwelling will be stronger, and can even reach the sea surface.

[24] Besides upwelling, tidal mixing itself can reduce SST in certain waters in summer. Numerical modeling shows that the SST off WCH is much lower than that in surrounding waters, even if upwelling does not reach the sea surface. This suggests that the formation of this low SST could be ascribed to two factors: frontal upwelling and tidal mixing.

[25] **Acknowledgments.** This study was supported by the Key Project of National Natural Science Foundation of China (Grant 40730842), the National Natural Science Foundation of China (Grant 40706016), the National 908 Project of China (Contract 908-02-01-03). The NSIPP AVHRR Pathfinder and Erosion Global 9km SST Climatology data were obtained from the Physical Oceanography Distributed Active Archive Center (PO.DAAC) at the NASA Jet Propulsion Laboratory, Pasadena, CA (http://podaac.jpl.nasa.gov).

References

Blumberg, A. F., and G. L. Mellor (1987), A description of a three-dimensional coastal ocean circulation model, in *Three Dimensional Coastal Ocean Models*, *Coastal Estuarine Sci.*, vol. 4, edited by N. S. Heaps, pp. 1–16, AGU, Washington, D. C.

Casey, K. S., and P. Cornillon (1999), A comparison of satellite and in situ-based sea surface temperature climatologies, *J. Clim.*, *12*, 1848–1863.

Chai, F., H. Xue, and M. Shi (2001), Upwelling east of Hainan Island (in Chinese), in *Oceanography in China*, vol. 13, edited by H. Xue, F. Chai, and J. Xu, pp. 129–137, China Ocean Press, Beijing.

Deng, S., H. Zhong, M. Wang, and F. Yun (1995), On the relationship between upwelling off Qionghai and fishery (in Chinese), *J. Oceanogr. Taiwan Strait*, *14*, 51–56.

Han, W., M. Wang, and K. Ma (1990), On the lowest surface water temperature area of China seas in summer: The upwelling along the east coast of Hainan Island (in Chinese), *Chin. J. Oceanol. Limnol.*, *21*, 267–275.

Hu, J. Y., H. Kawamura, and D. L. Tang (2003), Tidal front around the Hainan Island, northwest of the South China Sea, *J. Geophys. Res.*, *108*(C11), 3342, doi:10.1029/2003JC001883.

Li, L. (1990), A study on the summer upwelling in the shelf waters west to Zhujiang River mouth (in Chinese), *J. Oceanogr. Taiwan Strait*, *9*, 338–346.

Lü, X., F. Qiao, C. Xia, J. Zhu, and Y. Yuan (2006), Upwelling off Yangtze River estuary in summer, *J. Geophys. Res.*, *111*, C11S08, doi:10.1029/2005JC003250.

Qiao, F., Y. Yuan, Y. Yang, Q. Zheng, C. Xia, and J. Ma (2004), Wave induced mixing in the upper ocean: Distribution and application to a global ocean circulation model, *Geophys. Res. Lett.*, *31*, L11303, doi:10.1029/2004GL019824.

Simpson, J. H., and J. R. Hunter (1974), Fronts in the Irish Sea, *Nature*, *250*, 404–406.

Tang, D., H. Kawamura, M. Lee, and T. V. Dien (2003), Seasonal and spatial distribution of chlorophyll-*a* concentrations and water conditions in the Gulf of Tonkin, South China Sea, *Remote Sens. Environ.*, *85*, 475–483.

Xia, C., F. Qiao, Y. Yang, J. Ma, and Y. Yuan (2006), Three-dimensional structure of the summertime circulation in the Yellow Sea from a wave-tide-circulation coupled model, *J. Geophys. Res.*, *111*, C11S03, doi:10.1029/2005JC003218.

X. Lü, Institute of Oceanology, Chinese Academy of Sciences, Qingdao 266071, China.

F. Qiao, G. Wang, C. Xia, and Y. Yuan, First Institute of Oceanography, State Oceanic Administration, Qingdao 266061, China. (qiaofl@fio.org.cn)